

## Article

# Magnetic Molecularly Imprinted Chitosan Combined with a Paper-Based Analytical Device for the Smartphone Discrimination of Tryptophan Enantiomers

Abdelhafid Karrat <sup>1,2</sup>, Juan José García-Guzmán <sup>1</sup>, José María Palacios-Santander <sup>1,\*</sup>, Aziz Amine <sup>2,\*</sup>  
and Laura Cubillana-Aguilera <sup>1</sup>

- <sup>1</sup> Department of Analytical Chemistry, Institute of Research on Electron Microscopy and Materials (IMEYMAT), Faculty of Sciences, Campus de Excelencia Internacional del Mar (CEIMAR), University of Cadiz, Campus Universitario de Puerto Real, Polígono del Río San Pedro S/N, 11510 Puerto Real, Cádiz, Spain; hafidkarrat@gmail.com (A.K.); juanjo.garciaguzman@uca.es (J.J.G.-G.); laura.cubillana@uca.es (L.C.-A.)
- <sup>2</sup> Laboratory of Process Engineering & Environment, Faculty of Science and Technology, Hassan II University of Casablanca, B.P. 146, Mohammedia 28810, Morocco
- \* Correspondence: josem.palacios@uca.es (J.M.P.-S.); azizamine@yahoo.fr (A.A.)

**Abstract:** The separation of enantiomers plays a critical role in pharmaceutical development, ensuring therapeutic efficacy, safety, and patent protection. It enables the production of enantiopure drugs and enhances our understanding of the properties of chiral compounds. In this study, a straightforward and effective chiral detection strategy was developed for distinguishing between tryptophan (TRP) enantiomers. The approach involved the preparation of a magnetic molecularly imprinted chitosan (MMIC) for preparation of the sample, which was combined with a nitrocellulose membrane (a paper-based analytical device, PAD) integrated with D-TRP covalently grafted with polymethacrylic acid (PAD-PMA\_D-TRP). Discriminating between the TRP enantiomers was achieved using AuNPs as a colorimetric probe. Indeed, the presence of D-TRP rapidly induced the aggregation of AuNPs due to its strong affinity to PAD-PMA\_D-TRP, resulting in a noticeable change in the color of the AuNPs from red to purple. On the other hand, L-TRP did not induce any color changes. The chiral analysis could be easily performed with the naked eye and/or a smartphone. The developed method exhibited a detection limit of 3.3  $\mu\text{M}$ , and it was successfully applied to detect TRP in serum samples, demonstrating good recovery rates. The proposed procedure is characterized by its simplicity, cost-effectiveness, rapidity, and ease of operation.

**Keywords:** chitosan; magnetic molecularly imprinted polymer; discrimination of enantiomers; tryptophan; smartphone; paper-based analytical device



**Citation:** Karrat, A.; García-Guzmán, J.J.; Palacios-Santander, J.M.; Amine, A.; Cubillana-Aguilera, L. Magnetic Molecularly Imprinted Chitosan Combined with a Paper-Based Analytical Device for the Smartphone Discrimination of Tryptophan Enantiomers. *Biosensors* **2023**, *13*, 830. <https://doi.org/10.3390/bios13080830>

Received: 16 June 2023

Revised: 4 August 2023

Accepted: 15 August 2023

Published: 20 August 2023



**Copyright:** © 2023 by the authors. Licensee MDPI, Basel, Switzerland. This article is an open access article distributed under the terms and conditions of the Creative Commons Attribution (CC BY) license (<https://creativecommons.org/licenses/by/4.0/>).

## 1. Introduction

The majority of drugs, pharmaceuticals, and biologically active compounds are mixtures of chiral isomers, which have similar chemical and physical properties. However, in most cases, one isomer exhibits the desired biological and toxicological effects, while the other may be inactive or have different pharmacological effects [1,2]. For instance, the tragic incident in the early 1960s involving thalidomide revealed that only the (R)-enantiomer provided pain relief, while the (S)-enantiomer caused severe deformities in unborn children [3]. Another example is TRP, which has two enantiomers with distinct activities [4,5]. L-TRP is a vital component of proteins and is a precursor to melatonin and serotonin, which aids in sleep and improvements in mental health. On the other hand, D-TRP, a non-protein amino acid, does not participate in the metabolic pathways of living systems but it is commonly used in the synthesis of immunosuppressant and peptide antibiotics [6–8]. The importance of chiral molecules in the production of pharmaceutical and biologically active compounds has led to a significant demand for effective separation techniques to purify

chiral molecules from racemic mixtures. Molecular imprinting is a promising method of separation, as it relies on the spatial structure of the target molecules [9,10].

Molecularly imprinted polymers (MIPs) are cross-linked polymers formed through polymerization of a functional monomer (or co-monomers) in the presence of a template and a crosslinking agent [11,12]. Once the template is removed, recognition cavities are created within the polymer, which selectively recognize the target molecule in a mixture of compounds [13,14]. MIPs have found wide applications for various analytes such as viruses, bacteria, emerging pollutants, pharmaceutical drugs, and pesticides [15–17]. MIPs are largely used for the preparation of samples and the extraction of target analytes from complex matrices when combined with magnetic nanoparticles (MNPs) [18–20]. This combination offers several advantages. Firstly, it enables selective extraction of the target analytes from complex samples. Secondly, the magnetic properties of MNPs allow efficient and rapid extraction, as they can be easily manipulated and separated using a magnet. Additionally, MIPs provide a robust and reusable platform for selective extraction, as they can be regenerated and reused multiple times [21,22].

Chitosan, a polysaccharide derived from chitin, is particularly suitable for the development of MIPs due to its non-toxic, biocompatible, bioactive, and biodegradable properties. Its abundance of amino and hydroxyl groups allows it to react with various cross-linking agents for the preparation of MIPs [23–25]. In recent years, the use of gold nanoparticles (AuNPs) as optical labels has resulted in the development of numerous sensors and biosensors [26–28]. The simplicity of the synthesis of AuNPs and its intense red color, visible to the naked eye, make it a popular choice. However, research on colorimetric chiral discrimination using metal nanoparticles is limited, and a straightforward device for this purpose is yet to be developed. Consequently, constructing a reliable, user-friendly, sensitive, and high-throughput assay for determining the enantiomers of chiral substances still remains a challenge.

A PAD is a low-cost, portable, and disposable device that utilizes paper as the primary substrate for performing analytical tests. It integrates various components, such as sample application zones and detection zones for performing chemical or biological assays. The concept behind PADs is to leverage the properties of paper, such as its capillary action and porous structure, to facilitate fluid flow and reaction processes. The design typically involves creating channels on the paper's surface to direct the movement of the liquid samples and reagents [29,30]. PADs can be used for a wide range of applications, including clinical diagnostics, environmental monitoring, food safety testing, and drug detection. They often require minimal or no instrumentation, making them particularly suitable for resource-limited settings and point-of-need testing [31].

In this work, a magnetic molecularly imprinted chitosan (MMIC) was developed for the extraction of TRP and combined with a PAD for to discriminate between the enantiomers of TRP. The proposed PAD was based on a nitrocellulose membrane modified with D-TRP-grafted polymethacrylic acid (PMA\_D-TRP), successfully leading to good chiral separation using AuNPs as a colorimetric probe. The developed procedure holds promise for applications in pharmaceutical analysis, offering a reliable and user-friendly approach for chiral analysis.

## 2. Materials and Methods

### 2.1. Material and Apparatus

Chitosan,  $\text{FeCl}_3 \cdot 6\text{H}_2\text{O}$ ,  $\text{FeCl}_2 \cdot 4\text{H}_2\text{O}$  sulfuric acid ( $\text{H}_2\text{SO}_4$ ), L-TRP, D-TRP, methacrylic acid, ethylene glycol dimethylacrylate (EGDMA), azobisisobutyronitrile (AIBN), dimethylsulfoxide (DMSO), copper (II) chloride ( $\text{CuCl}_2$ ), acetic acid (AcH), polyphosphoric acid ( $\text{H}_3\text{PO}_4$ ), and boric acid ( $\text{H}_3\text{BO}_3$ ) were purchased from Sigma-Aldrich (Steinheim, Germany). Membrane filters (nitrocellulose, 0.45  $\mu\text{m}$ , 47 mm in diameter) were purchased from Sigma-Aldrich.

Scanning/transmission electron microscopy (TEM) images were acquired using FEI Nova NANOSEM 450 equipment (Thermo Fisher Scientific, Waltham, MA, USA)

(resolution = 1 nm). Fourier transform infrared (FT-IR) spectra were collected using aIR Affinity-1S spectrophotometer (Shimadzu, Japan) in the attenuated total reflectance (ATR) mode and across the range of 4000–500  $\text{cm}^{-1}$ . The UV absorption spectra were measured by a double beam UV/vis spectrophotometer (model T80+, PG Instruments, Wibtoft, Leicestershire, UK). The pictures for the discrimination of TRP were taken with an Android smartphone with a 13 MP camera. Nanopure water was prepared by a Wasser Lab Ultramatic Plus (Type I) system (Barbatáin, Navarra, Spain) and used in all experiments.

### 2.2. Synthesis of the Magnetite Nanoparticles

The synthesis of  $\text{Fe}_3\text{O}_4$  nanoparticles was carried out using the method described in [32]. In brief, a three-necked flask was prepared under a  $\text{N}_2$  atmosphere, and a solution containing 13.56 g of  $\text{FeCl}_3 \cdot 6\text{H}_2\text{O}$  and 4.96 g of  $\text{FeCl}_2 \cdot 4\text{H}_2\text{O}$  dissolved in 250 mL of distilled water was prepared. Subsequently, 20 mL of ammonium hydroxide was introduced into the flask, and the mixture was vigorously stirred for 40 min at 80 °C. The resulting  $\text{Fe}_3\text{O}_4$  nanoparticles were then collected using an external magnet and washed with distilled water to eliminate any residual chemicals. The obtained precipitate was finally dried at 50 °C in a vacuum oven.

### 2.3. Synthesis of Molecularly Imprinted Chitosan

The method of preparing MMIC was as follows. Initially, 100.0 mg of chitosan was dissolved in 10.0 mL of a 1.0% (v/v) aqueous acetic acid solution. At the same time, 6.0 mg of the TRP template molecules was added into the chitosan solution, followed by the addition of 100 mg of  $\text{Fe}_3\text{O}_4$  and stirred at room temperature for 4 h. Subsequently, 0.5 M sulfuric acid was added to the solution and stirred for 2 h. After that, the TRP template molecules were removed by an ethanol solvent. A magnetic non-imprinted chitosan (MNIC) was prepared following the same procedure, except for the addition of the template.

### 2.4. Synthesis of Gold Nanoparticles

Gold nanoparticles were synthesized according to our previous study [33]. Initially, a cylindrical glass vessel was placed in a water bath containing 1.25 mL of a 1.0 mM  $\text{HAuCl}_4$  aqueous solution. To ensure a consistent temperature, the sample vessel remained in the water bath at an ambient temperature throughout the process, as the local heating from sonication affected the solution's temperature. After 4 min of sonication, 250  $\mu\text{L}$  of an aqueous solution of 38.8 mM sodium citrate dihydrate was added to the vessel. This addition caused an immediate change in the solution's color to grey. Continuous sonication led to a subsequent transformation of the solution's color to dark red after 5.5 min, indicating the formation of the colloid AuNPs.

### 2.5. Synthesis of D-TRP-Grafted Polymethacrylic Acid (PMA\_D-TRP)

PMA\_D-TRP was prepared according to the following procedure: 20 mg of D-TRP was introduced into a beaker containing 50 mL of DMSO, followed by the addition of 700  $\mu\text{L}$  of MAA and 10 mL of EGDMA. Then 10 mg of  $\text{CuCl}_2$  was added to link the monomer to D-TRP covalently, and 3.3 mg of AIBN was used to initiate the process of polymerization. The blend was deaerated with nitrogen for 5 min and the reaction was carried out at 60 °C for 15 min using a domestic microwave. The material thus obtained was washed and dried in oven at 60 °C.

### 2.6. Preparation of the Paper-Based Analytical Device (PAD)

For this, 10 mg of the developed material (PMA\_D-TRP) was dispersed in 5 mL of nanopure water and filtrated under a vacuum to entrap the PMA\_D-TRP in the nitrocellulose membrane's pores (porosity: 0.45  $\mu\text{m}$ ). After filtration, the paper was dried in an oven for 15 min at 40 °C. The paper was then cut into small disks for further use and named PAD-PMA\_D-TRP.

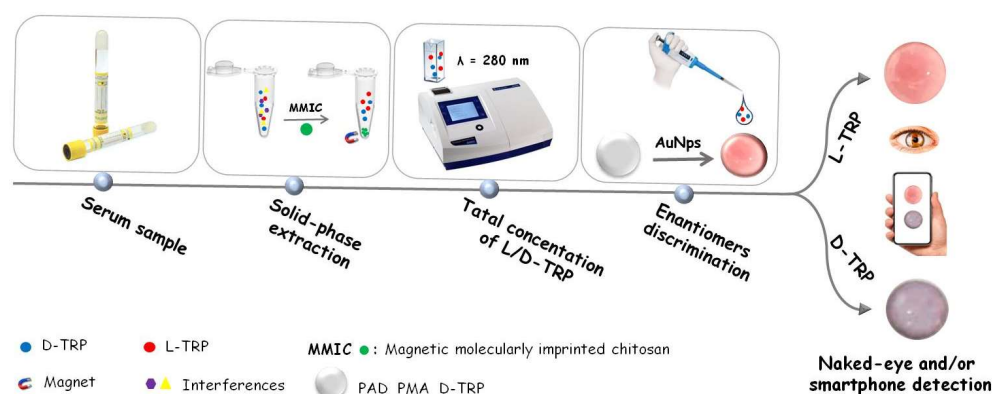
## 2.7. Adsorption Study

For this study, 10 mg of MMIC/MNIC was introduced into 1 mL of D-TRP with a concentration range of 30–320  $\mu\text{M}$ . The mixtures were shaken at a room temperature for 15 min. After the process of adsorption, the sorbent was separated by centrifugation at 1000 rpm for 2 min. The concentrations of the obtained supernatants were determined by the UV-spectrophotometer at a wavelength of 280 nm. The adsorption capacity ( $Q_e$ ) was calculated by Equation (1):

$$Q = \frac{C_i - C_e}{m} V \quad (1)$$

## 2.8. Solid-Phase Extraction Combined with Smartphone Detection

Solid-phase extraction is a versatile and effective technique of preparing samples that enables the selective extraction of the target analytes from complex sample matrices. In this work, the proposed MMIC was used as the sorbent in a solid-phase extraction technique for the total isolation of TRP. The task of discriminating between the TRP enantiomers was performed using the developed PAD-PMA\_D-TRP. The procedure was as follows. First, 10 mg of MMIC was introduced into an Eppendorf tube containing 1 mL of a TRP solution. The blend was shaken for 30 min at room temperature. After adsorption, the TRP was eluted with 1 mL of methanol and measured by UV spectroscopy at  $\lambda = 280 \text{ nm}$  to determine the total concentration of L/D-TRP. Then 10  $\mu\text{L}$  of the supernatant was added to the developed PAD-PMA\_D-TRP containing 40  $\mu\text{L}$  of the dispersed AuNPs, followed by the addition of 10  $\mu\text{L}$  of a Britton–Robinson (BR) buffer (0.04 M  $\text{H}_3\text{PO}_4$ , 0.04 M  $\text{AcH}$ , and 0.04 M  $\text{H}_3\text{BO}_3$ ) (pH4). After 25 min, the spots were measured with a smartphone (Scheme 1).



**Scheme 1.** Illustration of solid-phase extraction coupled with smartphone-based discrimination of L/D-TRP enantiomers.

## 3. Results and Discussion

### 3.1. Characterization Studies of $\text{Fe}_3\text{O}_4$ and MMIC

The FTIR technique was used to analyze the chemical composition and functional groups of the proposed materials (Figure 1A). The  $\text{Fe}_3\text{O}_4$  typically exhibited the absorption bands of O-H stretching vibration at 3200–3600  $\text{cm}^{-1}$  (adsorbed water) and a strong band around 550–650  $\text{cm}^{-1}$  corresponding to the Fe-O group. However, the MMIC material presented both the characteristic chitosan absorption bands, including O-H at 3200–3600  $\text{cm}^{-1}$ , C=O 1650  $\text{cm}^{-1}$ , and N-H around 1560  $\text{cm}^{-1}$ , and the characteristic bands of  $\text{Fe}_3\text{O}_4$  mentioned above. These results confirmed the modification of  $\text{Fe}_3\text{O}_4$  with chitosan.

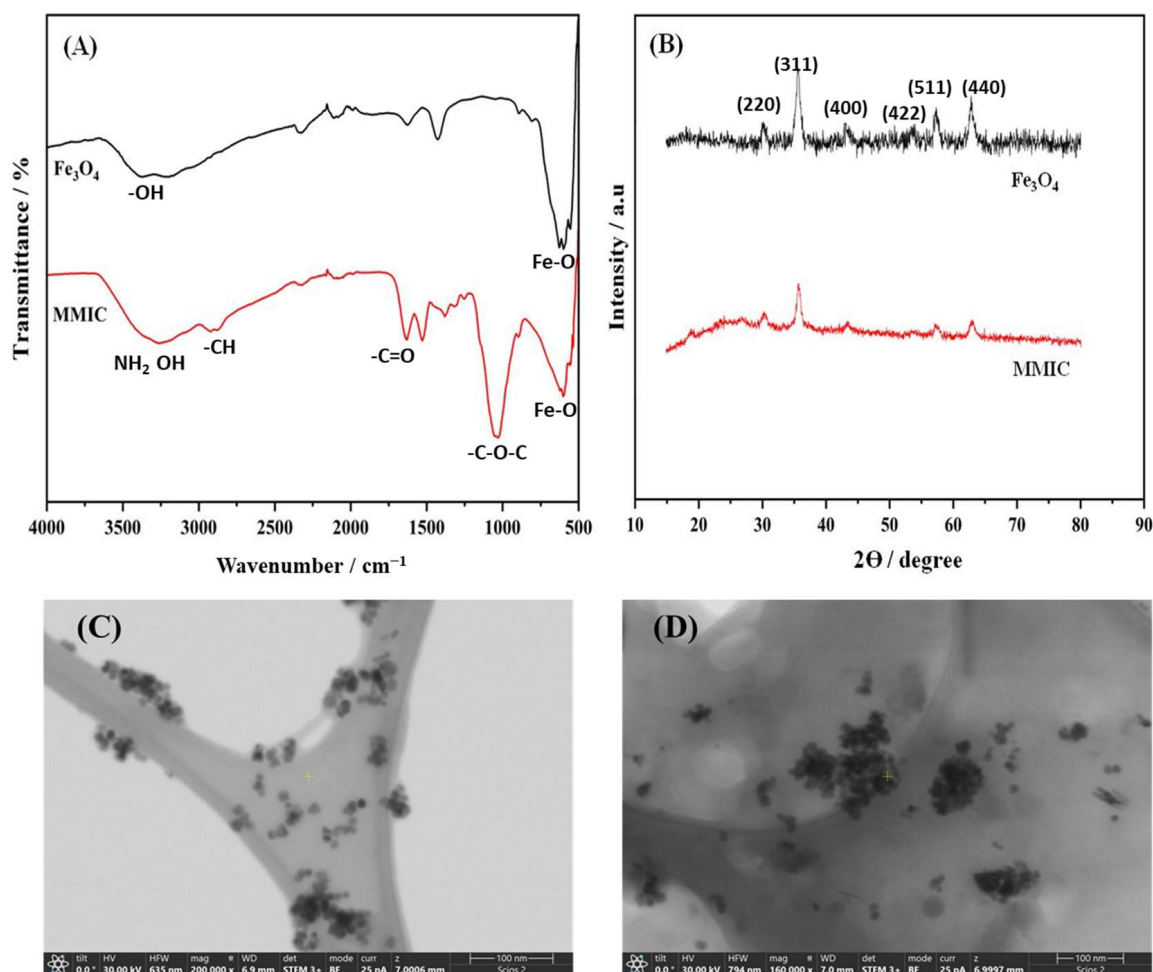


**Figure 1.** FTIR spectra (A) and XRD diffractograms (B) of Fe<sub>3</sub>O<sub>4</sub> and MMIC. (C,D) TEM images of Fe<sub>3</sub>O<sub>4</sub> and MMIC, respectively.

The XRD technique was also used to confirm the preparation of the materials (Figure 1B). Fe<sub>3</sub>O<sub>4</sub> exhibits a characteristic spinel crystal structure, with peaks typically observed at 2θ values around 30°, 35°, 43°, 57°, and 62°, corresponding to the (220), (311), (400), (511), and (440) crystal planes, respectively. These peaks corresponded well with the standard XRD data of magnetic Fe<sub>3</sub>O<sub>4</sub> (JCPDS No. 85-1436) [34]. When chitosan was decorated onto the Fe<sub>3</sub>O<sub>4</sub>, the XRD pattern showed changes in the peaks' intensities. These changes depended on the interaction between chitosan and Fe<sub>3</sub>O<sub>4</sub>.

TEM was used to characterize the size and morphological structure of the prepared materials, namely Fe<sub>3</sub>O<sub>4</sub> and Fe<sub>3</sub>O<sub>4</sub>-chitosan. The developed Fe<sub>3</sub>O<sub>4</sub> particles exhibited a mean diameter of approximately 12.03 ± 3.1 nm (n = 13) (see Figure 1C). However, MMIC (Figure 1D) showed dense particles due to the presence of the polymer, which modified a large number of the Fe<sub>3</sub>O<sub>4</sub> nanoparticles. These results strongly confirmed the successful modification of the magnetic nanoparticles with chitosan.

### 3.2. Transmission Electron Microscopy for AuNPs

TEM images were acquired to assess the behavior of AuNPs when exposed to D-TRP or L-TRP. As depicted in Figure 2A,B, the presence of D-TRP led to the aggregation of AuNPs. Conversely, in the presence of L-TRP, the AuNPs remained dispersed and exhibited a monodisperse distribution.

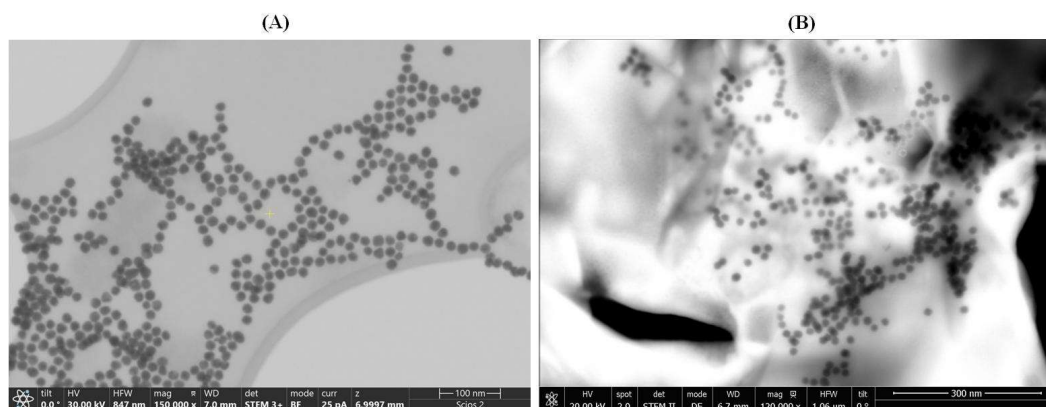


**Figure 2.** TEM images of AuNPs/L-TRP (A) and AuNPs/D-TRP (B). Micrographs were taken at different magnifications ( $\times 150,000$  and  $\times 120,000$ ) and in brightfield (BF) and darkfield (DF) field modes.

### 3.3. Adsorption Study

The adsorption study played a crucial role in the characterization of MIPs by providing insights into the binding capacity. It contributed to an understanding of the behavior of MIPs and aided in the development of cavities that were efficient and highly specific to the analyte.

The binding isotherms of D-TRP on the MMIC and MNIC at 25 °C are presented in Figure 3. As the concentration of D-TRP increased, both the MMIC and MNIC demonstrated higher binding capacities. However, due to the presence of multiple cavities, the MMIC exhibited a higher adsorption capacity compared with the MNIC. This observation was supported by the higher values of the imprinted factor, which represents the ratio of the adsorption capacity of MMIC to MNIC. The imprinted factor values ranged between 1.5 and 2, providing further evidence for the successful development of D-TRP cavities on the surface of the MMIC.

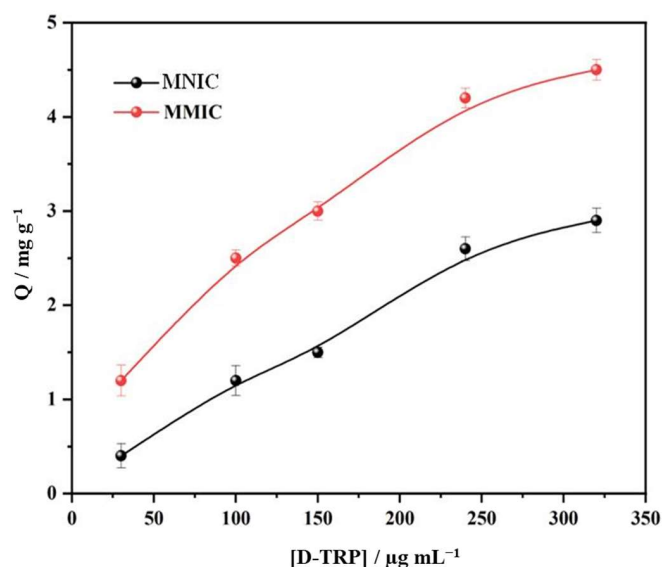
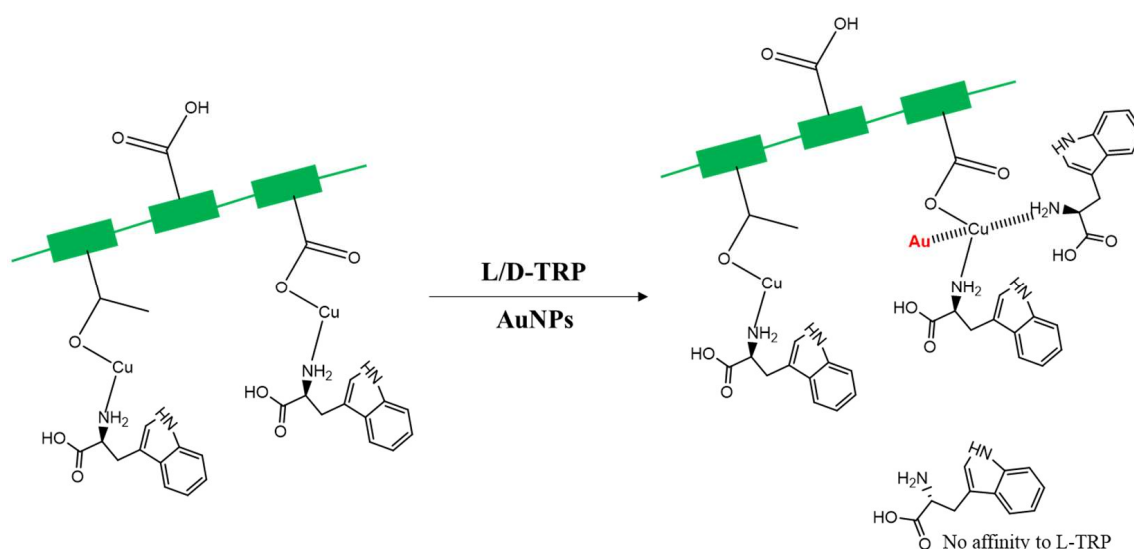


**Figure 3.** Adsorption isotherms of D-TRP on MMIC and MNIC at room temperature.

### 3.4. Discriminating between TRP Enantiomers

Discriminating between the two enantiomers of tryptophan is important for several reasons, including protein synthesis, the production of neurotransmitters, drug development, and understanding metabolism and health. In the present work, the discrimination

was performed after the extraction of total TRP using the developed MMIC. Indeed, a paper-based analytical device was developed for discriminating between the TRP enantiomers. This device is based on a membrane modified with polymethacrylic acid grafted with D-TRP (PAD-PMA\_D-TRP). For visual detection, AuNPs were used as colorimetric probes because of their sensitive aggregation with TRP. Indeed, the AuNPs changed color from red to purple through the aggregation phenomenon stimulated by TRP. The newly developed PAD-PMA\_D-TRP exhibited high affinity to D-TRP, providing a rapid aggregation of AuNPs. However, there was no interaction between PAD-PMA\_D-TRP and L-TRP, and thus the AuNPs maintained their red coloration (Scheme 2). This approach enabled the convenient discrimination of TRP enantiomers using a smartphone or even with the naked eye.



**Scheme 2.** Detailed mechanism of discriminating between TRP enantiomers.

### 3.5. Smartphone Detection

To enable on-site quantitative evaluation of the color change exhibited by AuNPs in the presence of TRP, we combined our PAD-PMA\_D-TRP with a smartphone. This allowed us to monitor alterations in the RGB values as the red color of the AuNPs transitioned to a purplish-blue upon the addition of TRP. The standard RGB scale uses whole-number values ranging from 0 to 255 to represent the intensity of each color channel: red, green, and blue. In this scale, [255, 255, 255] corresponds to pure white, while [0, 0, 0] represents absolute black [35–39]. By utilizing smartphone-based RGB detection, we were able to observe and record the changes in color. The RGB values were measured by Image J software 1.53t, and the difference between the red and blue (R-B) values was plotted against the concentration of TRP.

### 3.6. Optimization of the Detection Procedure

The volume of AuNPs, the pH conditions, and the time of color development are the most important parameters to be optimized in order to achieve an effective means of discriminating between TRP enantiomers.

As mentioned above, AuNPs were used as the colorimetric probe for the discrimination of TRP. Thus, the volume of AuNPs is a relevant parameter to be optimized. Figure 4A shows that 40  $\mu$ L of AuNPs was the most suitable volume to be added to the PAD-PMA\_D-TRP for the colorimetric discrimination of L-TRP and D-TRP enantiomers.

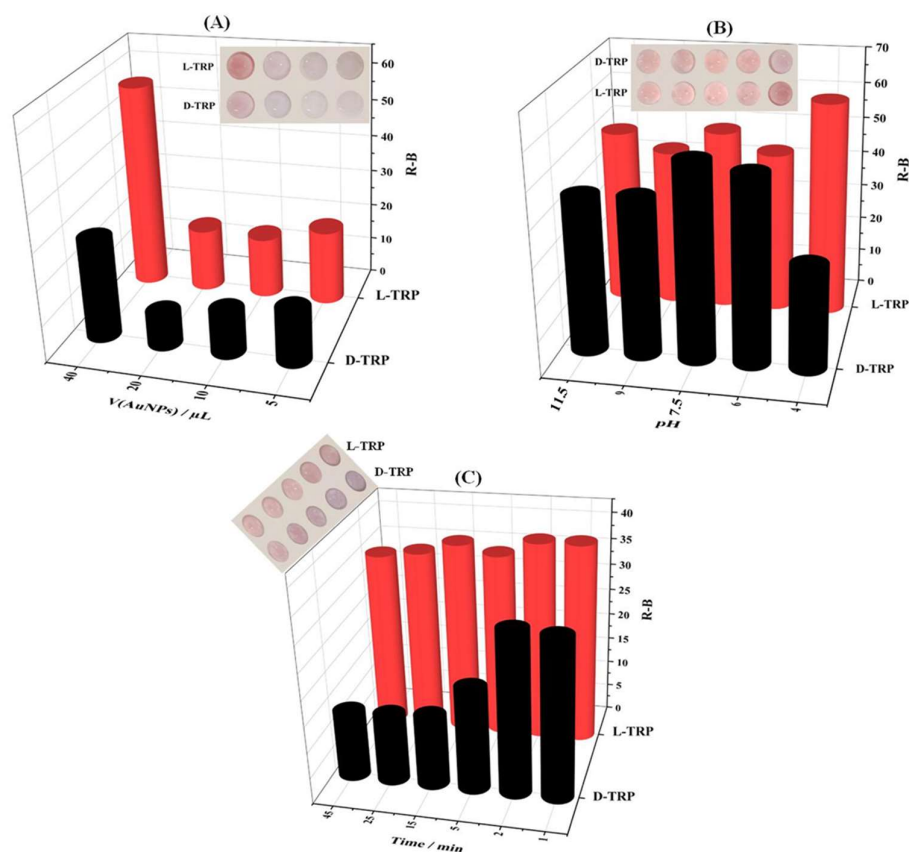


**Figure 4.** Effect of different parameters on the optimal discrimination of TRP enantiomers including (A) the volume of AuNPs (pH 4 and  $t = 25$  min), (B) the optimal pH (AuNPs = 40  $\mu$ L and  $t = 25$  min), and (C) the time of color development (AuNPs = 40  $\mu$ L, pH 4).

The aggregation of AuNPs depends on the pH of the solution (Figure 4B). Indeed, the pH effect of the BR buffer was studied in the pH range of 4–11.5. A good interaction between D-TRP and AuNPs was achieved at a pH value of 4. However, the L-TRP had no effect on the AuNPs' coloration. Furthermore, the effect of time on the ability to discriminate between the TRP enantiomers was also examined (Figure 4C). The addition of D-TRP showed a significant decrease in the R-B intensity compared with L-TRP. A significant difference between L-TRP and D-TRP was obtained at 25 min. Therefore, this time was utilized for subsequent experiments.

### 3.7. Calibration Curve

Figure 5A shows the calibration curves of D-TRP and L-TRP obtained using different concentrations ranging from 10 to 300  $\mu$ M. As shown in the photographs, the color of the PAD-PMA\_D-TRP color changed from pink to purple, and became more intense with an increasing concentration of D-TRP; thus, aggregation of the AuNPs occurred. However, with the addition of L-TRP, the PAD-PMA\_D-TRP showed no significant color change, indicating the low interaction between L-TRP and the developed material. To quantitatively evaluate the results, the color density was converted into the R-B color intensity. This relationship can be described by the equation  $R-B = -0.15X + 57$ , where X represents the concentration of the analyte. The correlation coefficient for this linear relationship was 0.986, indicating a strong association. The limit of detection (LOD) for D-TRP was determined to be 3.3  $\mu$ M, whereas the LOD for L-TRP could not be calculated due to the absence of a significant color change. These findings were based on three individual assays ( $n = 3$ ).

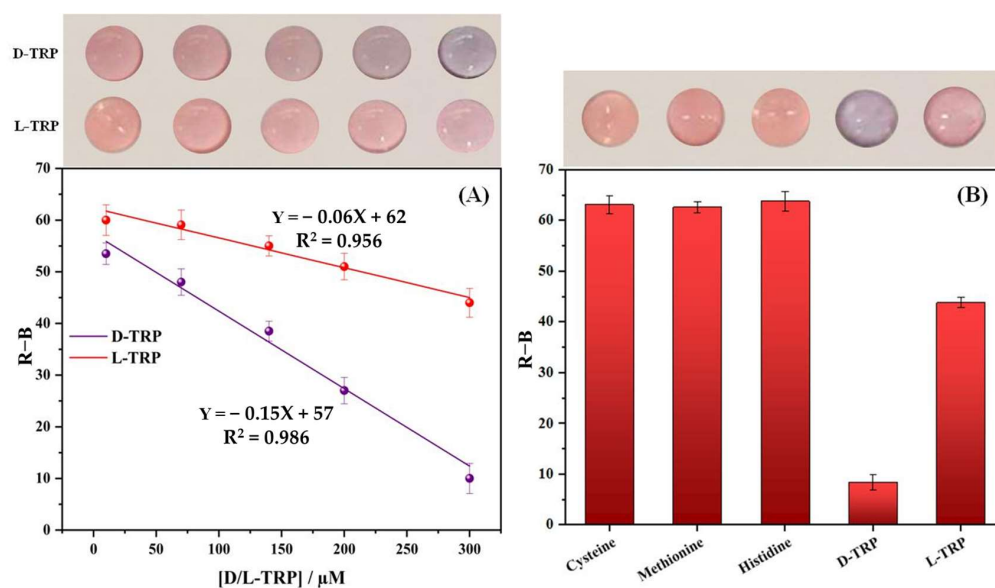


**Figure 5.** The change in color intensity (R-B) as a function of the concentration of D- and L-TRP between 10 and 300  $\mu\text{M}$  for the optimized assay (A). Selectivity of the developed PAD-PMA\_D-TRP device (B) ( $n = 3$ ).

### 3.8. Selectivity Study

A selectivity study plays a pivotal role in ensuring accurate and reliable analyses by identifying the target analytes and eliminating interference. The response of the newly developed PAD-PMA\_D-TRP was tested with other amino acids, including cysteine, methionine, histidine, and L-TRP. Figure 5B presents the results obtained under the optimal conditions. It is evident that only D-TRP exhibited a lower R-B response compared with the other amino acids. Notably, L-cysteine was found to cause aggregation of the AuNPs. However, the use of the MMIC in the sample's preparation effectively removed interferences such as L-cysteine thanks to its specific cavities, which were complementary only to TRP in terms of the shape, size, and functional groups. By combining the MMIC with the newly developed PAD-PMA\_D-TRP, successful discrimination of TRP enantiomers was achieved.

### 3.9. Enantioselective Measurement of L/D Tryptophan Mixtures

The primary objective was to investigate whether the discriminative sensing capability of AuNPs could be utilized for determining the enantiomeric percentage using the PAD-PMA\_D-TRP. Since TRP commonly exists as enantiomeric pairs, it is crucial to assess the influence of one enantiomer on the other. With the proposed approach, we were able to directly evaluate the performance of the PAD-PMA\_D-TRP in determining the percentage and confirming the enantioselective separation and purification of TRP in a racemic solution using AuNPs. Indeed, after the preparation of the samples using the developed MMIC, the concentration of L/D-TRP in the resulting supernatant could be determined by measuring the total concentration at 280 nm using UV spectroscopy. Subsequently, the percentage of each enantiomer was determined using the PAD-PMA\_D-TRP.

An interesting observation is related to the change in color from red to purple, which is dependent on the enantiomeric ratio. Figure 6 illustrates that the aggregation of AuNPs was selectively induced by D-TRP, leading to the precipitation of D-TRP with AuNPs. As a result, the excess of the other enantiomer remained in the solution, thereby enabling enantioseparation. The graph in Figure 6 demonstrates a linear decrease in the R-B intensity with an increasing enantiomeric percentage of D-TRP, ranging from 0% to 100%, indicating the optimized assay's ability to quantify the enantiomeric composition accurately.

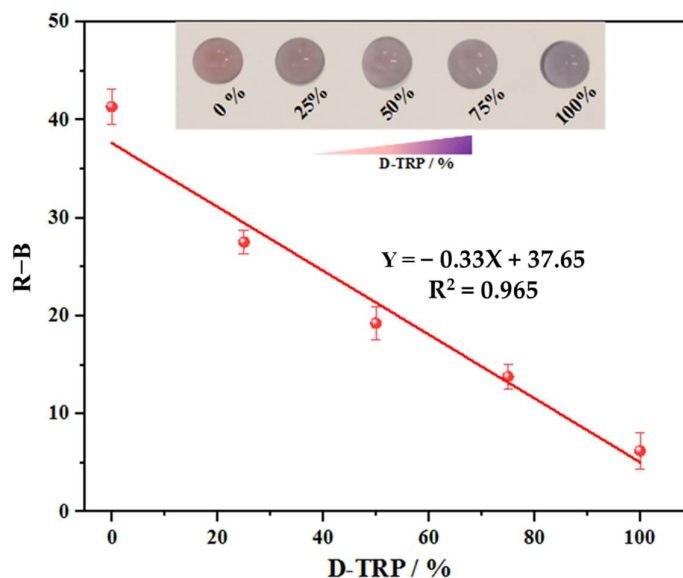


**Figure 6.** The linear decrease in the R-B response as a function of D-TRP (%) in the range from 0% to 100%. The total concentration of L/D-TRP was 300  $\mu$ M.

### 3.10. Real Sample

With the aim of using the proposed PAD-PMA\_D-TRP for a biological sample, it was utilized for the determination of D-TRP in a human serum sample. Samples spiked with 30 and 100  $\mu$ M of D-TRP were tested. The results are presented in Table 1 along with satisfactory recoveries of 88.6–106.4%. The obtained results confirmed the applicability of the developed device for the detection of D-TRP in real biological samples.

**Table 1.** The application of the proposed method for the determination of D-TRP in a spiked human serum sample.

Added ( $\mu$ M)	Found ( $\mu$ M)	Recovery (%)	RSD (%) *
30	26.5	88.6	3.4
100	106.4	106.4	2.7

\* n = 3.

## 4. Conclusions

The discrimination of enantiomers is necessary in order to understand their distinct biological activities, ensure the safety and efficacy of chiral drugs, and achieve analytical accuracy. This study presents a straightforward approach for the chirally selective sensing of TRP enantiomers using AuNPs as a colorimetric probe. The combination of MMIC with the developed PAD-PMA\_D-TRP enabled the chiral recognition of TRP. The detection of TRP enantiomers could be easily read with the naked eye and/or a smartphone. Remarkably, the proposed sensor demonstrated the capability to detect D-TRP in human serum, suggesting its potential as a valuable platform for analyzing real samples. This paper-based device represents the first example of a simple, cost-effective, and user-friendly platform for enantioselective sensing applications. The success of this application opens up new possibilities for designing innovative enantiosensing strategies in the future.

**Author Contributions:** A.K.: conceptualization, methodology, investigation, visualization, formal analysis, writing—original draft; J.J.G.-G.: validation, project administration, writing—reviewing and editing; J.M.P.-S.: supervision, conceptualization, funding acquisition, project administration, writing—review and editing; A.A.: supervision, conceptualization, project administration, writing—review and editing; L.C.-A.: funding acquisition, resources, writing—review and editing, visualization. All authors have read and agreed to the published version of the manuscript.

**Funding:** Abdelhafid Karrat gratefully acknowledges financial support from the Erasmus+ KA107 (EU) Program of the University of Cádiz (Spain), through “Servicio Español para la Internacionalización de la Educación” (SEPIE). The Spanish authors thank the Agencia Estatal de Investigación (AEI), the Ministerio de Ciencia e Innovación of Spain, and FEDER funds (EU) for the “Multibioanalysis” research project (Proyecto de Generación del Conocimiento, PID2021-122578NB-I00) financed by MCIN/AEI/10.13039/501100011033/FEDER, EU “ERDF: A way of making Europe”. They also thank “Plan Propio 2022–2023” from the University of Cadiz for providing funding through the “Acceso al uso de Servicios Centrales de Investigación. Financiación de Actividades” (Ref: SC2022–001) and the “Proyectos Noveles para Impulsar su Carrera Científica” (Ref: PR2022-025, SENSPOT) programs.

**Institutional Review Board Statement:** It should be noted that this study was carried out within the framework of a research project of the ‘Plan Estatal 2021’, entitled: “Development and validation of a multiparametric device for the continuous analysis of biomedical samples—MULTIBIOANALYSIS”. ‘Proyecto de Generación del Conocimiento’, PID 2021-122578NB-I00 financed by the Agencia Estatal de Investigación (AEI), Ministerio de Ciencia e Innovación of Spain, and FEDER (EU) funds “FEDER A way of making Europe”: MCIN/AEI/10.13039/501100011033. This project includes a research work applied to biological samples (human blood, plasma, and serum), such as the ones used in the present work. The study was conducted in accordance with the Declaration of Helsinki, and the aforementioned project and, consequently, the present study, in accordance with the Spanish regulation ‘Real Decreto 1090/2015, de 4 de diciembre, por el que se regulan los ensayos clínicos con medicamentos, los Comités de Ética de la Investigación con medicamentos y el Registro Español de Estudios Clínicos’, was approved by the Research Ethics Committee of Cadiz (Spain), on 12 May 2023, registry/protocol number 15.23, resolving that the aforementioned project, involving human samples, is viable, that it presents sufficient methodological rigor, that the evaluation of economic costs is correct, and that with respect to the ethical aspects, the project meets the necessary requirements of suitability of the protocol in relation to the objectives of the study.

**Informed Consent Statement:** Informed consent was obtained from the participant involved in this study to publish this paper.

**Data Availability Statement:** The data used to support the findings of this study are available from the corresponding author upon request.

**Acknowledgments:** The authors thank the TEP-243 research group for support regarding the ATR-FTIR spectra. Finally, the authors also acknowledge the Electron Microscopy and X-ray Diffraction and Fluorescence Divisions from Servicios Centrales de Investigación Científica y Tecnológica of the University of Cadiz (SC-ICYT-UCA) for their technical assistance during TEM and XRD measurements.

**Conflicts of Interest:** The authors declare no conflict of interest.

## References

1. Fanali, C. Enantiomers Separation by Capillary Electrochromatography. *TrAC Trends Anal. Chem.* **2019**, *120*, 115640. [[CrossRef](#)]
2. Makowski, K.; Mera, P.; Paredes, D.; Herrero, L.; Ariza, X.; Asins, G.; Hegardt, F.G.; García, J.; Serra, D. Differential Pharmacologic Properties of the Two C75 Enantiomers: (+)-C75 Is a Strong Anorectic Drug; (–)-C75 Has Antitumor Activity: Stereoselectivity of c75 enantiomers. *Chirality* **2013**, *25*, 281–287. [[CrossRef](#)]
3. Mori, T.; Ito, T.; Liu, S.; Ando, H.; Sakamoto, S.; Yamaguchi, Y.; Tokunaga, E.; Shibata, N.; Handa, H.; Hakoshima, T. Structural Basis of Thalidomide Enantiomer Binding to Cereblon. *Sci. Rep.* **2018**, *8*, 1294. [[CrossRef](#)]
4. Li, H.; Wang, L.; Yan, S.; Chen, J.; Zhang, M.; Zhao, R.; Niu, X.; Wang, K. Fusiform-like Metal-Organic Framework for Enantioselective Discrimination of Tryptophan Enantiomers. *Electrochim. Acta* **2022**, *419*, 140409. [[CrossRef](#)]
5. Jafari, M.; Tashkhourian, J.; Absalan, G. Chiral Recognition of Tryptophan Enantiomers Using Chitosan-Capped Silver Nanoparticles: Scanometry and Spectrophotometry Approaches. *Talanta* **2018**, *178*, 870–878. [[CrossRef](#)]
6. Liu, Y.; Li, Z.; Jia, L. Synthesis of Molecularly Imprinted Polymer Modified Magnetic Particles for Chiral Separation of Tryptophan Enantiomers in Aqueous Medium. *J. Chromatogr. A* **2020**, *1622*, 461147. [[CrossRef](#)] [[PubMed](#)]
7. Le Floc’h, N.; Otten, W.; Merlot, E. Tryptophan Metabolism, from Nutrition to Potential Therapeutic Applications. *Amino Acids* **2011**, *41*, 1195–1205. [[CrossRef](#)]
8. Platten, M.; Nollen, E.A.A.; Röhrig, U.F.; Fallarino, F.; Opitz, C.A. Tryptophan Metabolism as a Common Therapeutic Target in Cancer, Neurodegeneration and Beyond. *Nat. Rev. Drug Discov.* **2019**, *18*, 379–401. [[CrossRef](#)] [[PubMed](#)]
9. Maier, N.M.; Lindner, W. Chiral Recognition Applications of Molecularly Imprinted Polymers: A Critical Review. *Anal. Bioanal. Chem.* **2007**, *389*, 377–397. [[CrossRef](#)] [[PubMed](#)]

10. Karrat, A.; García-Guzmán, J.J.; Palacios-Santander, J.M.; Amine, A.; Cubillana-Aguilera, L. New Strategies for the Removal of Template from the Ion and Molecularly Imprinted Polymers: Application to the Fast and on-Site Cr(VI) Detection with a Smartphone. *Sens. Actuators B Chem.* **2023**, *386*, 133751. [[CrossRef](#)]
11. Díaz-Álvarez, M.; Martín-Esteban, A. Molecularly Imprinted Polymer-Quantum Dot Materials in Optical Sensors: An Overview of Their Synthesis and Applications. *Biosensors* **2021**, *11*, 79. [[CrossRef](#)] [[PubMed](#)]
12. Rutkowska, M.; Płotka-Wasyłka, J.; Morrison, C.; Wieczorek, P.P.; Namieśnik, J.; Marć, M. Application of Molecularly Imprinted Polymers in Analytical Chiral Separations and Analysis. *TrAC Trends Anal. Chem.* **2018**, *102*, 91–102. [[CrossRef](#)]
13. El Hani, O.; Karrat, A.; Digua, K.; Amine, A. Advanced Molecularly Imprinted Polymer-Based Paper Analytical Device for Selective and Sensitive Detection of Bisphenol-A in Water Samples. *Microchem. J.* **2023**, *184*, 108157. [[CrossRef](#)]
14. Villa, C.C.; Sánchez, L.T.; Valencia, G.A.; Ahmed, S.; Gutiérrez, T.J. Molecularly Imprinted Polymers for Food Applications: A Review. *Trends Food Sci. Technol.* **2021**, *111*, 642–669. [[CrossRef](#)]
15. Li, R.; Feng, Y.; Pan, G.; Liu, L. Advances in Molecularly Imprinting Technology for Bioanalytical Applications. *Sensors* **2019**, *19*, 177. [[CrossRef](#)]
16. Kadhem, A.J.; Gentile, G.J.; Fidalgo de Cortalezzi, M.M. Molecularly Imprinted Polymers (MIPs) in Sensors for Environmental and Biomedical Applications: A Review. *Molecules* **2021**, *26*, 6233. [[CrossRef](#)] [[PubMed](#)]
17. Madikizela, L.M.; Tavengwa, N.T.; Tutu, H.; Chimuka, L. Green Aspects in Molecular Imprinting Technology: From Design to Environmental Applications. *Trends Environ. Anal. Chem.* **2018**, *17*, 14–22. [[CrossRef](#)]
18. Ekmen, E.; Bilici, M.; Turan, E.; Tamer, U.; Zengin, A. Surface Molecularly-Imprinted Magnetic Nanoparticles Coupled with SERS Sensing Platform for Selective Detection of Malachite Green. *Sens. Actuators B Chem.* **2020**, *325*, 128787. [[CrossRef](#)]
19. Moya Betancourt, S.N.; Cámara, C.I.; Riva, J.S. Interaction between Pharmaceutical Drugs and Polymer-Coated Fe<sub>3</sub>O<sub>4</sub> Magnetic Nanoparticles with Langmuir Monolayers as Cellular Membrane Models. *Pharmaceutics* **2023**, *15*, 311. [[CrossRef](#)]
20. Chen, Q.; Liu, X.; Yang, H.; Zhang, S.; Song, H.; Zhu, X. Preparation and Evaluation of Magnetic Graphene Oxide Molecularly Imprinted Polymers (MIPs-GO-Fe<sub>3</sub>O<sub>4</sub>@SiO<sub>2</sub>) for the Analysis and Separation of Tripterine. *React. Funct. Polym.* **2021**, *169*, 105055. [[CrossRef](#)]
21. Poma, A.; Guerreiro, A.; Whitcombe, M.J.; Piletska, E.V.; Turner, A.P.F.; Piletsky, S.A. Solid-Phase Synthesis of Molecularly Imprinted Polymer Nanoparticles with a Reusable Template—“Plastic Antibodies”. *Adv. Funct. Mater.* **2013**, *23*, 2821–2827. [[CrossRef](#)]
22. Krupadam, R.J.; Patel, G.P.; Balasubramanian, R. Removal of Cyanotoxins from Surface Water Resources Using Reusable Molecularly Imprinted Polymer Adsorbents. *Environ. Sci. Pollut. Res.* **2012**, *19*, 1841–1851. [[CrossRef](#)]
23. Zouaoui, F.; Bourouina-Bacha, S.; Bourouina, M.; Jaffrezic-Renault, N.; Zine, N.; Errachid, A. Electrochemical Sensors Based on Molecularly Imprinted Chitosan: A Review. *TrAC Trends Anal. Chem.* **2020**, *130*, 115982. [[CrossRef](#)]
24. Mulyasuryani, A.; Prananto, Y.P.; Fardiyah, Q.; Widwastuti, H.; Darjito, D. Application of Chitosan-Based Molecularly Imprinted Polymer in Development of Electrochemical Sensor for p-Aminophenol Determination. *Polymers* **2023**, *15*, 1818. [[CrossRef](#)] [[PubMed](#)]
25. Kharroubi, M.; Bellali, F.; Karrat, A.; Bouchdoug, M.; Jaouad, A. Preparation of Teucrium polium extract-loaded chitosan-sodium lauryl sulfate beads and chitosan-alginate films for wound dressing application. *AIMS Public Health* **2021**, *8*, 754–775. [[CrossRef](#)]
26. He, S.; Liu, D.; Wang, Z.; Cai, K.; Jiang, X. Utilization of Unmodified Gold Nanoparticles in Colorimetric Detection. *Sci. China Phys. Mech. Astron.* **2011**, *54*, 1757–1765. [[CrossRef](#)]
27. Chang, C.-C.; Chen, C.-P.; Wu, T.-H.; Yang, C.-H.; Lin, C.-W.; Chen, C.-Y. Gold Nanoparticle-Based Colorimetric Strategies for Chemical and Biological Sensing Applications. *Nanomaterials* **2019**, *9*, 861. [[CrossRef](#)]
28. Chahri, I.; Karrat, A.; Mohammadi, H.; Amine, A. Development of a New Route for the Immobilization of Unmodified Single-Stranded DNA on Chitosan Beads and Detection of Released Guanine after Hydrolysis. *Molecules* **2023**, *28*, 2088. [[CrossRef](#)]
29. Noviana, E.; Ozer, T.; Carrell, C.S.; Link, J.S.; McMahon, C.; Jang, I.; Henry, C.S. Microfluidic Paper-Based Analytical Devices: From Design to Applications. *Chem. Rev.* **2021**, *121*, 11835–11885. [[CrossRef](#)]
30. Martinez, A.W.; Phillips, S.T.; Whitesides, G.M.; Carrilho, E. Diagnostics for the Developing World: Microfluidic Paper-Based Analytical Devices. *Anal. Chem.* **2010**, *82*, 3–10. [[CrossRef](#)]
31. Fu, L.-M.; Wang, Y.-N. Detection Methods and Applications of Microfluidic Paper-Based Analytical Devices. *TrAC Trends Anal. Chem.* **2018**, *107*, 196–211. [[CrossRef](#)]
32. Afzali, M.; Mostafavi, A.; Shamspur, T. A Novel Electrochemical Sensor Based on Magnetic Core@shell Molecularly Imprinted Nanocomposite (Fe<sub>3</sub>O<sub>4</sub>@graphene Oxide@MIP) for Sensitive and Selective Determination of Anticancer Drug Capecitabine. *Arab. J. Chem.* **2020**, *13*, 6626–6638. [[CrossRef](#)]
33. Cubillana-Aguilera, L.M.; Franco-Romano, M.; Gil, M.L.A.; Naranjo-Rodríguez, I.; Hidalgo-Hidalgo de Cisneros, J.L.; Palacios-Santander, J.M. New, Fast and Green Procedure for the Synthesis of Gold Nanoparticles Based on Sonocatalysis. *Ultrason. Sonochemistry* **2011**, *18*, 789–794. [[CrossRef](#)]
34. Li, G.; Jiang, Y.; Huang, K.; Ding, P.; Chen, J. Preparation and Properties of Magnetic Fe<sub>3</sub>O<sub>4</sub>-Chitosan Nanoparticles. *J. Alloy. Compd.* **2008**, *466*, 451–456. [[CrossRef](#)]
35. Upadhyay, Y.; Bothra, S.; Kumar, R.; Sahoo, S.K. Smartphone-Assisted Colorimetric Detection of Cr<sup>3+</sup> Using Vitamin B<sub>6</sub> Cofactor Functionalized Gold Nanoparticles and Its Applications in Real Sample Analyses. *ChemistrySelect* **2018**, *3*, 6892–6896. [[CrossRef](#)]

36. Karrat, A.; Amine, A. Paper-Based Analytical Device for One-Step Detection of Bisphenol-A Using Functionalized Chitosan. *Chemosensors* **2022**, *10*, 450. [[CrossRef](#)]
37. Rezazadeh, M.; Seidi, S.; Lid, M.; Pedersen-Bjergaard, S.; Yamini, Y. The Modern Role of Smartphones in Analytical Chemistry. *TrAC Trends Anal. Chem.* **2019**, *118*, 548–555. [[CrossRef](#)]
38. Xu, J.; Wang, J.; Li, Y.; Zhang, L.; Bi, N.; Gou, J.; Zhao, T.; Jia, L. A Wearable Gloved Sensor Based on Fluorescent Ag Nanoparticles and Europium Complexes for Visualized Assessment of Tetracycline in Food Samples. *Food Chem.* **2023**, *424*, 136376. [[CrossRef](#)]
39. Xu, J.; Guo, S.; Jia, L.; Zhu, T.; Chen, X.; Zhao, T. A Smartphone-Integrated Method for Visual Detection of Tetracycline. *Chem. Eng. J.* **2021**, *416*, 127741. [[CrossRef](#)]

**Disclaimer/Publisher's Note:** The statements, opinions and data contained in all publications are solely those of the individual author(s) and contributor(s) and not of MDPI and/or the editor(s). MDPI and/or the editor(s) disclaim responsibility for any injury to people or property resulting from any ideas, methods, instructions or products referred to in the content.